Experimental test and sensitivity analysis of performance parameters of a solar humidification–dehumidification system

David Saldivia[a], Rodrigo Barraza[b,*], Danilo Estay[b], Patricio Valdivia[c], Mauricio Reyes[b], Jesús García[b]

[a]*School of Photovoltaics and Renewable Energy Engineering, University of New South Wales, Sydney, NSW 2052, Australia, email: d.saldiviasalazar@unsw.edu.au*
[b]*Department of Mechanical Engineering, Universidad Técnica Federico Santa Maria, Av. Vicuña Mackenna 3939, Santiago, Chile, emails: rodrigo.barraza@usm.cl (R. Barraza), danilo.estay@usm.cl (D. Estay), mauricio.reyes@usm.cl (M. Reyes), jesus.garcia@usm.cl (J. García)*
[c]*Department of Electrical Engineering, Universidad Técnica Federico Santa Maria, Av. Vicuña Mackenna 3939, Santiago, Chile, email: patricio.valdivial@usm.cl*

ABSTRACT

Sun-powered desalination technologies, such as humidification–dehumidification (HDH), are an attractive alternative to provide freshwater in remote high-radiation climate conditions. In this work, an experimental and numerical study is presented for a solar HDH unit operating with a closed air-open water configuration with water-heated solar collectors. The numerical model shows a good agreement with experimental data for both temperature and distillate production. A new performance parameter, so-called distillate-to-irradiance ratio (DIR), is introduced, which is specifically designed to characterise solar thermal desalination systems. This parameter takes into account both solar collection and desalination processes and could be complemented with the conventional gained output ratio (GOR = $M_d \lambda/Q_u$), which involves the distillate M_d with the heat required to distillate Q_u. The validated model is used to determine the relevant operational parameters and how they influence the DIR throughout a sensitivity analysis. Feedwater to air mass flow rate ratio (MR) and solar radiation are the key parameters to predict DIR and distillate production. For the specific conditions, a maximum of DIR = 0.44 kg/kWh for a global radiation of 1,000 W/m² and a MR = 2 was found. Finally, short- and long-term correlations based on environmental conditions were developed to easily estimate the desalination potential in specific locations.

Keywords: Solar energy; Humidification–dehumidification; Solar desalination; Distillation

1. Introduction

Water and energy are interdependent resources that have become increasingly important over recent years due to their environmental, economic, and social implications. Both resources are related because producing one of them through any available technology requires resources of the other. Thus, integration between energy, water, and climate change has increased research efforts in recent years [1–3]. Today, "Clean water and sanitation" and "Affordable and clean energy" are two of the United Nations' 17 Sustainable Development Goals [4]. Currently, primary freshwater resources around the world are threatened due to overexploitation and contamination. According to United Nations, in 2015, 29% of the global population has no access to drinking water services, and over

* Corresponding author.

2 billion people are living in countries with excess water stress, which means a strong probability of future water scarcity [5]. These conditions are present in the northern Chilean regions, and some specific zones have also shown that the water requirement exceeds the water supply [6]. Nevertheless, Chile has developed a great advantage during the last years. There is an impressive growth in renewable energy, due to its vast solar energy potential in the northern zone. In 2019, 8.2% of gross power generation was produced by solar energy [7]. Consequently, the coupling of desalination technologies with solar energy to achieve a sustainable social-economic system is attractive.

On the other hand, desalination is a promising alternative to provide clean water in desert conditions and isolated areas. There are two leading families of desalination technologies, according to their energy input source and how they separate the solutes. These categories are grouped into electromechanical and thermal methods. The first category includes reverse osmosis and electrodialysis technologies. Conventional alternatives within the second category include multistage flash and multi-effect distillation (MED). Novel thermal techniques are membrane distillation, humidification–dehumidification (HDH), and solar stills, among others [8]. The thermal methods are suitable for using solar-thermal, geothermal, or waste heat [3]. There are various reviews available matching renewable energy and desalination, and precisely, regarding solar desalination [9–11]. Among thermal desalination technologies, humidification–dehumidification (HDH) is a promising alternative for producing water in a decentralised small-scale manner. This system can operate autonomously, is suitable to work with solar energy or other low-grade heat sources, has low operation costs, and does not require a highly-qualified personal for its operation and maintenance. Besides, HDH has a low recovery ratio (RR < 5%), resulting in low brine discharge impact and less scaling problem inside the equipment [12,13].

The literature reviews show plenty of experience using HDH around the world, and in multiple configurations. Narayan et al. [12] presented a literature review of HDH technology showing two major classifications between HDH systems. The first classification relies on the type of water and air loops, which can be open or closed, being closed-air-open-water (CAOW) and closed-water-open-air (CWOA) two of the most used configurations. The second classification is based on the energy source: water-heating, air-heating, or both (air and water heating) with separated heaters or dual-purpose collectors. Water heating is the preferred alternative because it is a mature technology with a higher efficiency. Several experimental facilities have been built over the last decade aiming to improve the technologies performance by testing different configurations, including different types of solar collectors and humidifiers [12,14–20]. One of the main conclusions obtained is that the humidifier is a key component of the system. The most common solution is the packed bed humidifier due to its higher humidification efficiency. Many packed materials have been tested, including wooden materials, textile materials, ceramic Raschig rings, aluminium sheets, plastic pad, and wire mesh, among others [12,21]. The specific production with these materials ranges from 0.7 kg/ m^2 d for torn trees [22], up to 6–8 kg/m^2 d for plastic pads [23]. In addition to the previously mentioned studies, the humidification process has not been widely analysed theoretically and numerically. Kloppers and Kröger [24] made a theoretical analysis for a wetted-wall tower, based on methods derived from cooling tower models, such as Merkel, Popper, and ε-NTU methods. The literature that includes a detailed numerical model of packed-bed humidifier by means of the analysis of heat and mass transfer phenomena and considering the vertical profiles for both water and air mass flow rates is scarce. In this research, a CAOW HDH unit with solar water heating is studied. A detailed numerical model of the system is developed including the packed bed humidifier, dehumidifier, and solar heating system.

The conventional parameter used to compare different thermal desalination systems in term of its performance is the gained output ratio (GOR). It defines the effectiveness in the energy use, calculated through the ratio between the energy required to vaporise the distilled water and the actual energy absorbed by the system. In the case of solar desalination, the GOR may not wholly capture the performance of the system, and additional parameters are required to assess the whole system. Some studies have also widely used a relationship between daily water production and the specific area of the solar collection. However, this term does not take into account the incident solar energy and the conversion efficiency to thermal energy. Researchers presented by Rajaseenivasan and Srithar [25,26] tested dual purpose solar collector using water and air coupled with a CWOA scheme with two different humidifiers, a packed bed and bubble column humidifiers. Their production achieved ranged from 12.4 to 20.6 kg/m^2 d (GOR = 1.8–3.3), for a dual-purpose collector and featuring an additional air heater. Yildirim and Solmuş [27] reported theoretical results where it is shown that water heating has a greater impact on improving the yield of an HDH system as opposed to air heating, given the higher heat capacity of water. Air heating has a less significant effect on the yield of the system. However, if water and air are heated together, the productivity of the system is improved. Regarding experimental tests, experimental facilities have been built to study the improvement methods aiming to increase the thermal performance. These methods rely on additional components, or the use of different configurations. Gang et al. [28] tested the use of multiple humidifier–dehumidifiers stages, reaching a GOR of 2.6 for maximum temperature in the humidifier of 85°C. Muthusamy and Srithar [29] used turbulence generators inside the humidifier, reporting a 45% increase in production compared to conventional humidifiers. Moreover, several hybrid configurations have been proposed and studied with variable success, such as HDH-solar still [30], HDH with industrial waste heat recovery [31], heat pump-driven HDH [32], HDH-flash evaporation [33], HDH-solar dryer [34] or HDH-desiccant air conditioner [35]. However, all these modifications make the system prohibitively expensive or technically complex to be implemented in rural areas.

In Chile, a few investigations in solar desalination have been performed, which is focused on numerical simulations

rather than experimental studies. Directly driven solar energy MED systems have been analysed [8,36], and integrated poly-generation systems that combine concentrating solar power [37,38], and PV technologies with desalination [39,40]. A numerical study regarding a solar thermal membrane distillation system has also been studied [41,42]. This investigation shows an experimental and numerical evaluation of a solar HDH unit, which is the first facility of its kind in Chile.

This study presents an experimental facility, a complete numerical model, a sensitivity analysis, and a performance parameter optimization of a desalination system based on a one-stage solar CAOW HDH unit. Some of the novelties of this work are: (i) This is the first experimental facility of this kind located in Chile and provides valuable data to understand the behavior of this technology. (ii) The validated numerical model is used to run a novel sensitivity analysis allowing to identify the main variables that influence the performance and define the main non-dimensional parameters to characterize the system. (iii) A novel index is introduced, the distillate-to-irradiance ratio (DIR), to reflect in the proper performance of solar desalination systems, complementing the conventional GOR, which does not reflect adequately the more efficient operational point, as is shown in this work. Finally, correlations for short-term (hourly) and long-term (yearly) production were developed, which are useful for a quick potential assessment of HDH desalination in the location of interest.

2. Experimental facility

The desalination unit shown in Fig. 1 is located in the Renewable Energy Laboratory (LER) of the Universidad Técnica Federico Santa María (33°02′22.42″ S 71°29′09.1″ W) in Chile. The experimental HDH desalination unit has a close air loop, and an open water loop (CAOW), where the water is indirectly heated using solar energy. The experimental facility is shown in Fig. 1a and b, and

somepreliminary results have been previously presented by Hernández et al. [43]. The cold feedwater enters through the dehumidifier (stream 1 in Fig. 1a). It cools down the pure water that is condensing over the fins of the dehumidifier. The preheated feedwater leaves the dehumidifier (2) and enters the heating plate heat exchanger, where the feedwater is heated by the solar thermal collector water loop (5). The hot feedwater is sprayed inside the humidifier (3), mixing the water with the air while heating it. The heated air increases its capacity to retain moisture and absorbs a fraction of water. The remaining water leaves the desalination unit (4). At the same time, the humid air exits the humidifier through a duct (8) and is directed to the dehumidifier, where the air is cooled down, condensing purified water. The dry air (7) is then recirculated back to the humidifier.

The humidifier is a cylindrical tank that operates in a similar manner to an evaporative tower, humidifying the air. A packing bed is installed to increase the surface area favouring the heat and mass transfer processes between the air and water. Table 1 presents the main parameters of the humidifier.

The dehumidifier is an unmixed-crossflow-finned heat exchanger. The water flows through the tubes and the humid air contacts the fins where the freshwater condenses. Table 2 shows the constructive parameters of the dehumidifier.

The heating heat exchanger is a parallel flow plate heat exchanger that transfers the thermal energy collected by the solar thermal collector loop to the feedwater. Four Flate-plate type solar collectors are used. An experimental test was made to determine the characteristic parameters of the solar collectors ($F_R U_L$ and $F_R(\tau\alpha)$). Freshwater is circulated through the collectors to avoid scaling due to the salty feedwater. Table 3 presents the main parameters of the heating unit HX and the solar thermal collectors.

Instruments are installed in the sample points of the HDH facility, as indicated in Fig. 1, numbers included. Temperature is measured using Resistance Temperature
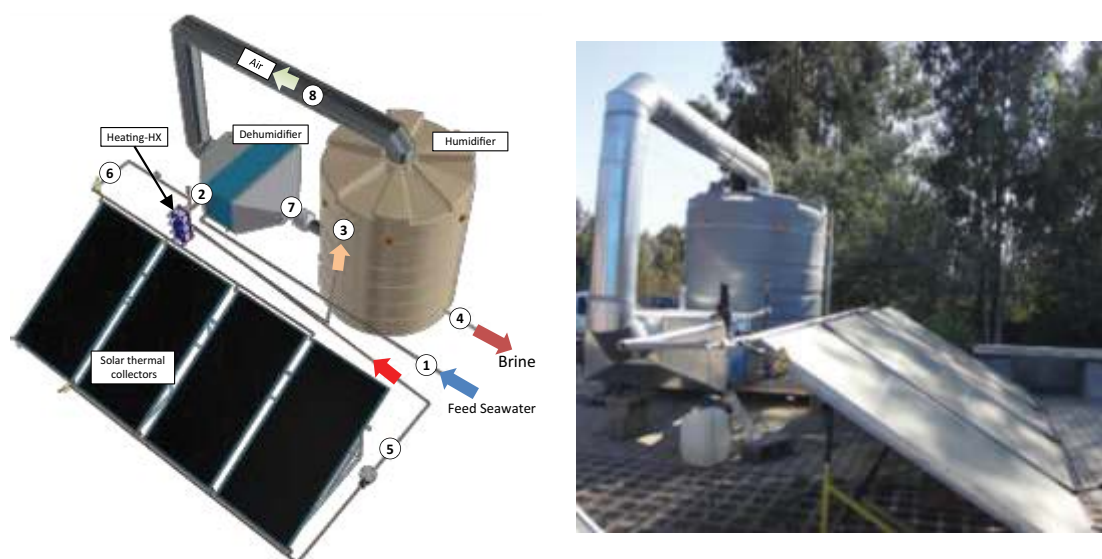

Fig. 1. HDH unit: (a) schematic design and (b) experimental facility.

Table 1
Main parameters of the humidifier

Parameter	Value
Total diameter, D_h, mm	1,660
Total height, H_h, mm	2,100
Packing height, H_{hp}, mm	600
Packing diameter, D_{hp}, mm	1,640
Packing specific area, a_h, m²/m³	226
Nozzle type	PJ24
Packing material	PVC type C-12

Table 2
Main parameters of the dehumidifier

Parameter	Value
Number of rows, N_r	12
Number of passes, N_p	4
Heat exchanger length, L, mm	330
Heat exchanger width, W, mm	1,100
Heat exchanger height, H, mm	470
Outer tube diameter, D_o, mm	12
Tube thickness, e_p, mm	1.24
Fin separation, b_j, mm	3.00
Thickness fin, e_f, mm	0.33
Tube rugosity, μ, mm	0.0015
Tube material	Copper
Fin material	Aluminium

Table 3
Main parameters of the solar collection subsystem

Parameter	Value
Heat exchanger model	Alfa Laval, T2-BFG/12H
Number of plates, N_{hx}	12
Active heat exchanger area, A_{hx}, m²	0.78
Solar collector model	YAZAKI, SC-V1020
Solar collector type	Flat plate, double glass
Effective collector area, A_c, m²	1.91
$F_R U_L$ – experimental, W/m²K	4
$F_R(\tau\alpha)$ – experimental	0.62

Detectors (RTD). The RTDs are installed at inlets and outlets of each component within the HDH system, therefore the temperature measurement is redundant at each point. The feedwater stream volume flow rate is measured, and so is the thermal solar collector flow loop. The volume flow rate of the air loop is determined by measuring the air velocity in different locations. In the air loop, temperature and relative humidity are measured before and after the humidifier and dehumidifier. A portable weather station measures environmental conditions such as temperature, relative humidity, and wind speed. The solar radiation received by the solar collector is measured using a Pyranometer with the same inclination of the solar collectors. Table 4 shows the technical data of the instrumentation used to register the operational data of the HDH system.

3. Numerical model

A numerical model for the CAOW water-heated solar-HDH unit was developed by means of Engineering Equation Solver (EES) [44]. The performance of the HDH unit is evaluated using mass and energy balances, and mass and heat transfer equations, based on the preliminary numerical model presented by Hernández et al. [43]. Three loops are studied: feedwater, humid air, and solar collector loops. Individual models for the humidifier, dehumidifier, and solar collector water loop are developed as subprograms, which allows studying each component separately. The different modules are coupled in the main program identifying the relations between inputs and outputs. Steady-state conditions are assumed for this model, considering that solar radiation changes slowly during the day, and only small variations are present in the internal energy of the HDH unit components.

3.1. Humidifier

The humidifier is fed by high pressure warmed water (4 barg), which is sprayed onto the humidifier. These small water drops fall over a packing bed, while at the same time a stream of air circulates in counterflow. The fed air is saturated but cold. As the air moves up, it encounters the falling spray of warm water, absorbing heat and increasing its capacity to carry water. Consequently, the humidity ratio of the air is increased. Fig. 2 shows the control volume that defines this process, which has a height of dZ and a cross-sectional area equal to the humidifiers cross-sectional area A_h. Schematically, all the water inside this volume is grouped on the left side, while all the humid air is grouped on the right side. The interface area is given by the differential active surface area represented by $dA = a\ dV = a\ a_h\ dZ$, where a is the packing specific area per volume unit, and dV is the differential control volume. The water is cooled down by heat and mass transfer effects. Heat transfer occurs due to temperature differences between water and air. The cooling process is also related to the energy extracted to vaporise a fraction of the sprayed inlet water. Mass transfer occurs due to the difference in the concentration of water (humidity) between the air-water interface (saturated) and the air, which enters at saturated conditions but gains heat increasing its capacity to retain humidity.

The mass water balance, discretised along the vertical axis of the humidifier, is defined by the change on the humidity ratio in the element [Eq. (1)], and the mass transfer rate from water to air is defined by Eq. (2).

$$\frac{dm_w}{dZ} = \frac{d\omega}{dZ} m_a \tag{1}$$

$$\frac{dm_w}{dZ} = h_D \left(a \times a_h \right) \left(\omega_s - \omega \right) \tag{2}$$

Table 4
Instrumentation used in the experimental facility

| Device	Type/model	Range	Accuracy
Temperature sensor, °C	RTD PT100	(–40)–(125)	±0.1
Volume flow meter, l/min	Bopp & Reuther	0–10	±0.1
Pressure sensor, bar	Khöne	0–10	±0.2
Hygrometer	AZ 8723 (digital)	0%–100%	±0.1%
Pyranometer, W/m²	Kipp & Zonen SP Lite2	0–2,000	50
Anemometer, m/s	PCE Instruments PCE-009	0.2–20	±0.1
Hygrometer and thermometer (ambient)	iButton	HR: 0%–100%	HR: ±0.04%
		–10°C – +85°C	±0.5°C
Weather station [temperature, relative humidity (HR),	PCE Instruments	–40°C – +65°C	±0.1°C
wind speed (WS), atmospheric pressure]	PCE-FWS 20	10% – 90% (HR)	1% (HR)
		0–180 km/h (WS)	0.1 m/s (WS)
		700–1,100 kPa	0.1 kPa
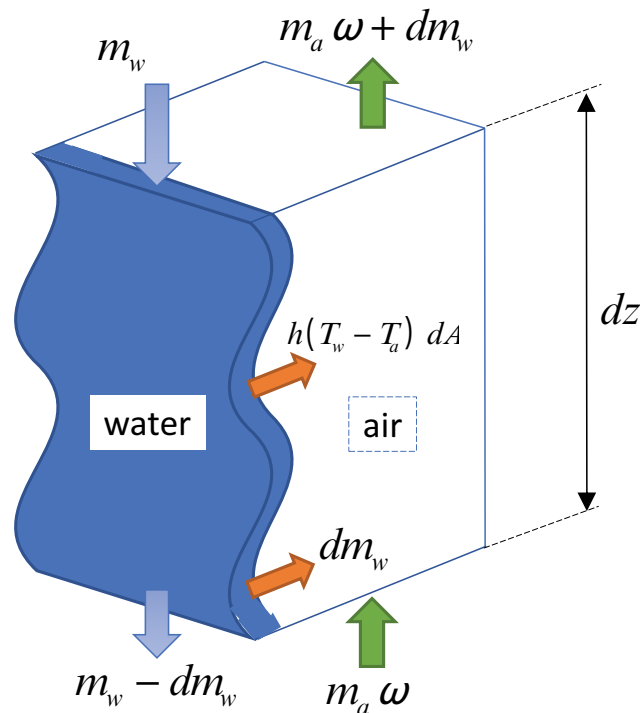
Fig. 2. Control volume of the humidifier. Schematically, the water is placed on the left side, and the air is placed on the right side.

where m is the mass flow rate, T is temperature, and ω represents the humidity ratio. The subscripts are a for dry air and w for water. ω_s is the humidity ratio at the air-water interface, which is assumed at saturated condition and h_D represents the mass transfer coefficient. The air and water energy balance at the interface, and the heat transfer equation are presented in Eqs. (3)–(5).

$$\frac{d(m_a i_{aw})}{dZ} = \frac{d(m_w i_w)}{dZ} = \frac{dQ_m}{dZ} + \frac{dQ_c}{dZ} \tag{3}$$

$$\frac{dQ_m}{dZ} = i_v \cdot \frac{dm_w}{dZ} \tag{4}$$

$$\frac{dQ_c}{dZ} = h_c \left(a \times a_h \right)\left(T_w - T_a \right) \tag{5}$$

where Q_c and Q_m represent energy flows associated with convection and mass transfer, respectively, i is the specific enthalpy, and h_c is the heat transfer coefficient between a film of falling water and the ascending air. The enthalpies are a function of temperature and pressure. The air mass flow rate is considered dry air and is a fixed value over all the humidifier. The wet air enthalpy (i_{aw}) calculation includes the moisture content of the air, as presented in Eq. (6).

$$i_{aw} = i_a + \omega i_v \tag{6}$$

where i_a is the dry air enthalpy and i_v is the enthalpy of the saturated vapor at air temperature. The heat transfer process is modelled using the correlation presented by Nellis and Klein [45], which is shown in Eq. (7).

$$\mathrm{Nu} = \begin{cases} \dfrac{0.3387 \cdot \mathrm{Re}^{1/2} \cdot \mathrm{Pr}^{1/3}}{\left[1 + \left(\dfrac{0.0468}{\mathrm{Pr}} \right)^{2/3} \right]^{1/4}} & \text{laminar flow} \\[6pt] 0.0296 \cdot \mathrm{Re}^{4/5} \cdot \mathrm{Pr}^{1/3} & \text{mixed and turbulent flow} \end{cases} \tag{7}$$

The Reynolds, Prandtl, and Nusselt numbers are calculated based on the humidifier diameter and height, using the average temperature inside each element. The mass transfer coefficient is calculated using the Lewis factor as presented in Eq. (8) [24], which relates to mass and heat transfer:

$$\mathrm{Le} = \frac{k}{\rho h_D c_p} \tag{8}$$

The Lewis factor is calculated according to Bosnjakovic [46] and shown in Eq. (9).

$$\mathrm{Le} = 0.865^{2/3} \frac{\left(\dfrac{\omega_s + 0.622}{\omega + 0.622} - 1 \right)}{\ln \left(\dfrac{\omega_s + 0.622}{\omega + 0.622} \right)} \tag{9}$$

All thermodynamic properties (including enthalpies) are calculated at the mean element conditions using standard correlations available in EES [44], which are based on Hyland and Wexler [47].

3.2. Dehumidifier

The dehumidifier (condenser) is modelled as an unmixed crossflow heat exchanger. The humid warmed air flows through the outside of the finned surface. Meanwhile, the cold feedwater flows through the pipes. Two phenomena preheat the feedwater, the air is cooled down, and some of the water in the air is condensed. Thus, the humid air transfers energy to the cold feedwater before it enters the heating HX. The main characteristic of the dehumidifier is the variation of enthalpy and specific heat of the air due to the change in water content, which does not allow an analysis of the heat exchanger as a whole. Therefore, the heat exchanger is discretised as a function of the number of passes. The heat transfer analysis is made using ε-NTU method for each pass j as described by Nellis and Klein [45]. The incoming air enters at the first column (the upper one) where it transfers heat with the coldest feedwater. The global heat transfer coefficient (U_j) is obtained by applying a thermal resistance analysis that includes the waterside (including a fouling factor), the airside, the pipes, and the finned surface.

It is necessary to know the specific heat (c_p) and the capacitance (C) for both the water and air in order to apply the ε-NTU method. Eq. (10) presents these properties for the cold water flow, and Eq. (11) presents them for the humid air flow.

$$C_{w,j} = m_w c_{p,w,j} = m_w \frac{di_{w,j}}{dT_{w,j}} = m_w \left(\frac{i_{w,\mathrm{out},j} - i_{w,\mathrm{in},j}}{T_{w,\mathrm{out},j} - T_{w,\mathrm{in},j}} \right) \tag{10}$$

$$C_{a,j} = m_a c_{p,\mathrm{aw},j} = m_a \frac{di_{\mathrm{aw},j}}{dT_{a,j}} = m_a \left(\frac{i_{\mathrm{aw},\mathrm{out},j} - i_{\mathrm{aw},\mathrm{in},j}}{T_{a,\mathrm{out},j} - T_{a,\mathrm{in},j}} \right) \tag{11}$$

All the enthalpies for air are calculated considering its moisture content, using Eq. (6). Finally, the heat transferred in each discrete element may be obtained with Eq. (12), while the temperature increase of feedwater is calculated with Eq. (13).

$$Q_{d,j} = \in Q_{d,\mathrm{max}} \tag{12}$$

$$T_{w,\mathrm{out},j} = T_{w,\mathrm{in},j} + \frac{Q_{d,j}}{C_{w,j}} \tag{13}$$

where $Q_{d,j}$ is the heat transferred in the j-th pass. The outlet air temperature and distillate production may be obtained using Eqs. (14) and (15), respectively.

$$Q_{d,j} = m_a \left(i_{\mathrm{aw},\mathrm{out},j} - i_{\mathrm{aw},\mathrm{in},j} \right) \tag{14}$$

$$m_{d,j} = m_a \left(\omega_{a,\mathrm{in},j} - \omega_{a,\mathrm{out},j} \right) \tag{15}$$

3.3. Solar collector and heating heat exchanger

The collector is characterized by the well-known Hottel–Whillier equation, Eq. (16), the equation is used as presented by Duffie and Beckman [48]. The energy balance in the solar collector loop is shown in Eq. (17).

$$Q_u = A_C F_R \left(G_T (\tau \alpha) - U_L \left(T_{f,\mathrm{in}} - T_{\mathrm{amb}} \right) \right) \tag{16}$$

$$Q_u = m_f c_p \left(T_{f,\mathrm{out}} - T_{f,\mathrm{in}} \right) \tag{17}$$

where the subscript f indicates the water flow inside the collector. The heat absorbed by the water (Q_u) in the solar collector loop is transferred to the feedwater in the heating heat exchanger, which is modelled using the standard ε-NTU method for parallel flow heat exchangers, using similar equations described in section 3.2.

3.4. Performance parameter

The main model output is distillate production (M_d), the inlet and outlet temperature in each component and overall performance parameters, such as GOR and DIR, which are calculated using Eqs. (18)–(19).

$$\mathrm{GOR} = \frac{M_d \lambda}{Q_u} \tag{18}$$

$$\mathrm{DIR} = \frac{M_d}{G_T A_T} = \frac{M_d}{G_T \left(A_C + A_{\mathrm{PV}} \right)} \tag{19}$$

DIR is a suggested performance parameter used to reflect the performance behaviour of solar desalination systems. GOR is the standard thermal desalination parameter, however, it only considers the desalination process, this parameter does not take into account the solar collection process. It could lead to misunderstanding conclusions about the operational performance of a solar desalination system. For example, if the heat exchanger has a high operational temperature, the GOR increases, but this also decreases the thermal collector efficiency, which means a lower use of the available solar incident irradiation.

The suggested DIR is an overall parameter that involves both the collection and desalination subprocesses.

Other relevant parameters to describe the HDH operation are the mass flow rate ratio (MR) and the recovery ratio (RR). MR is the ratio between the inlet feedwater mass flow rate (m_{fw}) and the air mass flow rate, as shown in Eq. (20). RR presents the ratio between the distillate mass flow rate and the feedwater mass flow rate, as indicated in Eq. (21).

$$MR = \frac{m_{fw}}{m_a} \tag{20}$$

$$RR = \frac{M_d}{m_{fw}} \tag{21}$$

3.5. Validation

The numerical model is validated using experimental data collected during February and March 2020 from the experimental HDH facility. The operating parameters are shown in Table 5.

The environmental variables, including tilted solar radiation, ambient temperature, and inlet feedwater temperature are shown in Fig. 3. This day was selected because it offered a high radiation throughout the day.

Fig. 4 shows a comparison between experimental and estimated temperatures for the humidifier (a), dehumidifier (b), heating HX (c), and solar collectors (d). Each component

Table 5
Operating parameters of the experimental plant

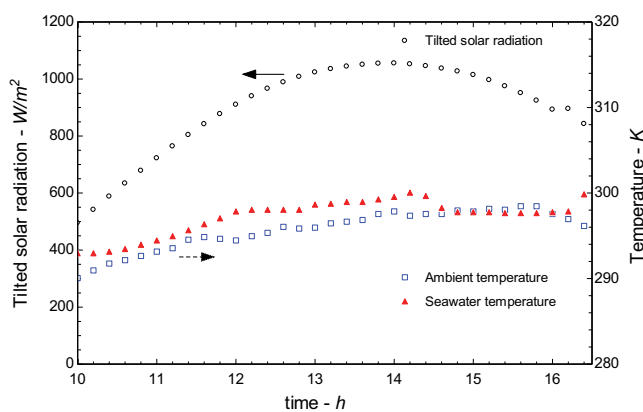| Parameter	Operating value
Feedwater mass flow rate m_{fw}, kg/h	270
Dry air mass flow rate m_a, kg/h	600
Collector water mass flow rate m_c, kg/h	470
Water pressure in pumps, P_{fw}, barg	4

Fig. 3. Environmental variables and tilted solar radiation on March 1st, 2020.

is shown separately, comparing the experimental and numerical results. Most of the experimental values (point) are close to the identity line, which indicates an accurate prediction, and all the values present an error margin under ±2 K of (represented by the upper and lower dashed lines). Therefore, the model shows a close match to the experimental data retrieved.

Fig. 5 shows the comparison between the experimental accumulated distillate production and the simulation results for March. The experimental results show that the desalination unit produced close to 11.2 L of freshwater between 11:00 and 16:30 h. The measured average global radiation was 5.2 kWh/m² for this operation period. In the desalination system, the DIR is 0.27 kg/kWh and represents a GOR of 0.37. The peak freshwater production with the actual configuration is 2.3 kg/h. The production rate (the curve slope) of the experimental and model output are in agreement.

4. Analysis and discussion

4.1. Sensitivity analysis

A sensitivity analysis using the Sobol method [49] is made to determine the most critical variables that affect the distillate production. The input data is generated with Saltelli's pseudo-random sample generation method [50]. Ten variables are performed, and 1,000 samples are made, running a total of 22,000 different simulations. The two main output parameters of the Sobol method are first-order indexes S_1 and S_{T1}. S_1 measures the influence of each individual variable i, eliminating the influence of inter-variable effects. The sum $\sum S_{1,i}$ is always lesser than one, being the remaining part the influence of inter-variable effects. S_{T1} shows the total effect of each variable (including inter-variable effects), hence it can be greater than one (because the effect of S_{ij} from variables i and j is counted twice in weights S_{Ti} and S_{Tj}). Table 6 shows the tested variables, their range of operation, and their first order indexes. The indexes are calculated for distillate production (M_d), GOR, and DIR.

According to Table 6, the more influencing variables for distillate production are Global radiation (0.38), the number of solar collectors (0.30) and the feedwater mass flow rate (0.06). In the case of GOR, the main influencing variables are feedwater mass flow rate (0.61), packing specific area (0.13) and air mass flow rate (0.07). Finally, for DIR, the main variables are feedwater mass flow rate (0.37), packing specific area (0.20), and air mass flow rate (0.12).

Additionally, a second-order analysis is done, to determine the grade of influence between two specific input variables, S_{ij}. The five variables with major indexes are chosen (feedwater and air mass flow rate, solar irradiation, packing specific area, and the number of collectors) and are shown in Table 7. The most substantial inter-variable influence over the distillate production is that between solar irradiation and the number of collectors (0.05), which is an expected result because both variables define the available energy for the solar-HDH system.

A multi-variable regression could be developed with the data retrieved. A linear regression is plotted using the
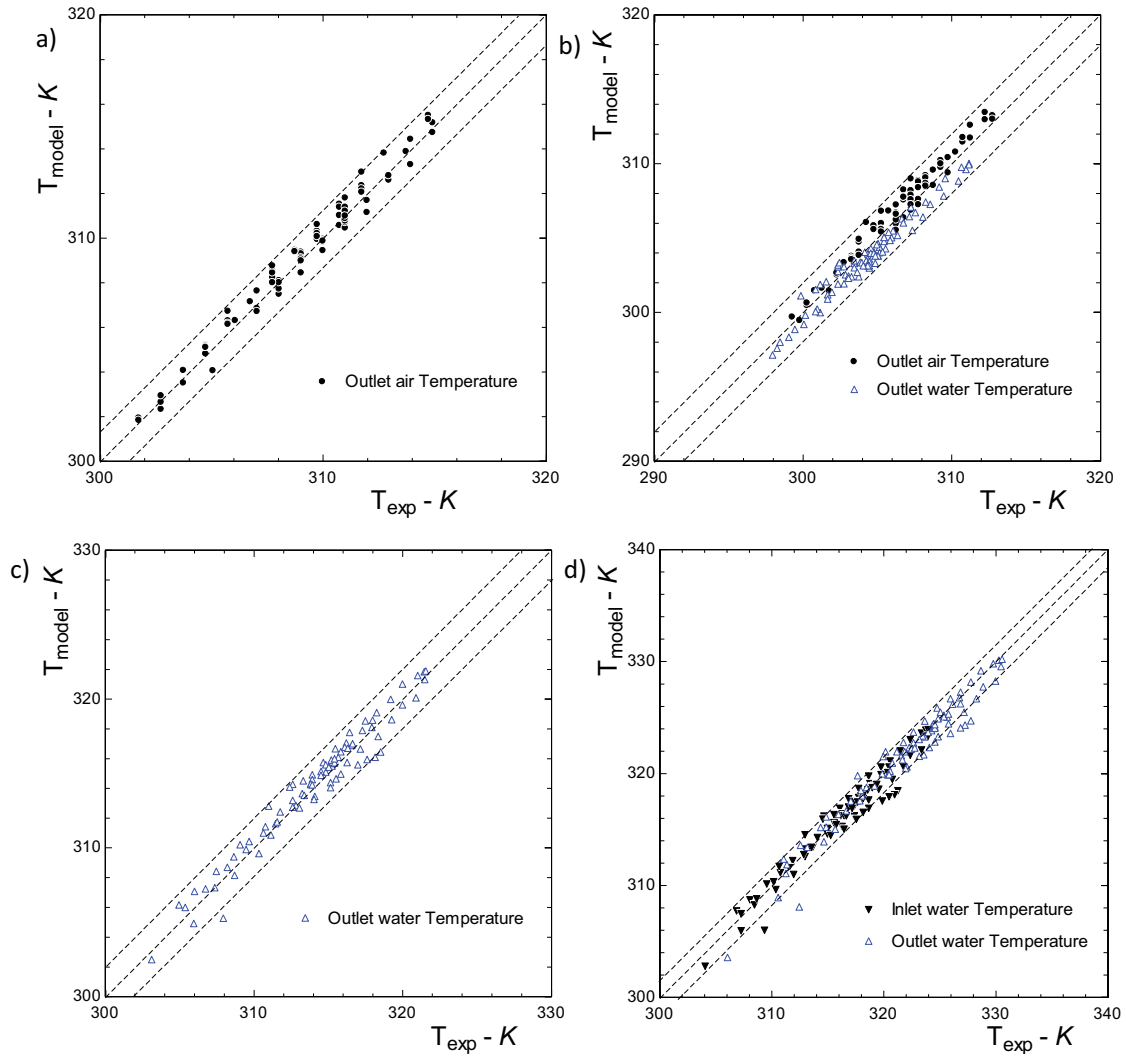
Fig. 4. Experimental and numerical temperatures. (a) Humidifier, (b) dehumidifier, (c) heating HX, and (d) solar loop.
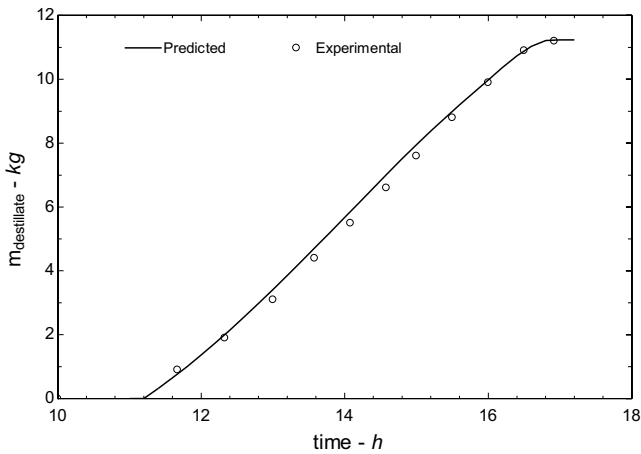

Fig. 5. Comparison between accumulated distillate production of experimental data and the simulation results.

five significant variables and the most critical inter- influence variables ($G_T N_C$) for M_d, GOR, and DIR, which are shown in Fig. 6. Feedwater inlet temperature (T_{fw}) has a considerable influence over the GOR and is included in its correlation. Additional parameters do not significantly increase the quality of the regression. Eqs. (22)–(24) show linear regression for M_d ($R^2 = 0.86$), GOR ($R^2 = 0.82$), and DIR ($R^2 = 0.65$), respectively.

$$M_d = -0.23 - 15.8 m_{fw} + 9.82 m_a - 3.57 \times 10^{-4} G_T + 4.16 \times 10^{-3} a_h - 0.049 N_C + 5.70 \times 10^{-4} G_T N_C \tag{22}$$

$$GOR = -1.42 - 4.55 m_{fw} + 1.66 m_a + 6.48 \times 10^{-5} G_T + 6.65 \times 10^{-3} T_{fw} + 6.65 \times 10^{-4} a_h + 1.83 \times 10^{-3} N_C + 6.98 \times 10^{-6} G_T N_C \tag{23}$$

$$DIR = 0.25 - 1.78 m_{fw} + 1.05 m_a + 6.89 \times 10^{-5} G_T - 4.04 \times 10^{-4} a_h - 4.6 \times 10^{-3} N_C + 3.15 \times 10^{-6} G_T N_C \tag{24}$$

Table 6
Sensitivity analysis results using Sobol method for 10 HDH parameters

Parameter	Symbol, unit	Range of variation	Distillate production, M_d (kg/h)		Gained output ratio, GOR (–)		Distillate-to-irradiance ratio, DIR (kWh/kg)	
			S_1	S_{T1}	S_1	S_{T1}	S_1	S_{T1}
Feedwater mass flow rate	m_{fw}, kg/h	200–600	0.06	0.11	0.61	0.64	0.37	0.47
Air mass flow rate	m_a, kg/h	200–600	0.03	0.05	0.07	0.12	0.12	0.18
Collector water mass flow rate	m_c, kg/h	400–1,000	<0.01	0.01	<0.01	0.01	<0.01	<0.01
Global radiation in tilt plane	G_T, W/m²	100–1,000	0.38	0.53	0.02	0.06	0.06	0.01
Ambient temperature	T_{amb}, K	5–30	<0.01	0.02	<0.01	0.01	0.06	0.07
Feedwater inlet temperature	T_{fw}, K	5–30	<0.01	0.02	0.02	0.07	<0.01	0.06
Humidifier diameter	D_h, m	0.5–3.0	<0.01	0.01	<0.01	0.03	0.01	0.02
Humidifier height	H_h, m	0.3–2.0	<0.01	0.02	0.01	0.04	0.02	0.04
Packing specific area	a_h, m²/m³	50–400	0.04	0.07	0.13	0.19	0.20	0.25
Number of solar collector	N_C	1–20	0.30	0.42	0.03	0.06	0.02	0.11
Total	–	–	0.81	1.26	0.87	1.23	0.86	1.30

First-order indexes are presented for distillate production, gained output ratio and distillate-to-irradiance ratio.

Table 7
Sensitivity analysis results using Sobol method for five HDH parameter

Parameter	m_{fw}	m_a	G_T	a_h	N_C
Feedwater mass flow rate, m_{fw}	–	0.00	0.00	0.00	0.01
Air mass flow rate, m_a	0.00	–	0.01	0.00	0.01
Global radiation in tilt plane, G_T	0.00	0.01	–	0.02	0.05
Packing specific area, a_h	0.00	0.00	0.02	–	0.02
Number of solar collector, N_C	0.00	0.01	0.05	0.02	–

Second-order indexes for five more influential variables over distillate production are presented.

4.2. Mass flow rate influence

The feedwater and air mass flow rates influence over HDH output is analysed. The geometrical and operational parameters are set as those of the experimental facilities. Besides, the environmental parameters are defined as G_T = 1,000 W/m², T_{fw} = 20°C, and T_{amb} = 20°C. Fig. 7 shows an optimum distillate production, which is almost independent of the air mass flow rate when the feedwater mass flow rate is in the range of 50–125 kg/h. The maximum distillate mass flow rate is 3.3 kg/h when the feedwater mass flow rate is 75 kg/h, and the air mass flow rate is 50 kg/h. Two phenomena may explain the optimum. On the one hand, a minimal feedwater mass flow rate diminishes the heat and mass transfer inside the humidifier and dehumidifier. On the other hand, a reduced feedwater mass flow rate generates a higher operating temperature in the collector HX. Consequently, a higher operating temperature in the solar collector is achieved and the collector efficiency is diminished. The air mass flow rate has a similar effect. A higher air mass flow rate means more capacity to transport water, and when the feedwater flow is small, it may not be enough to heat the air. Thus, the distillate production is diminished due to a smaller humidity ratio differences in the system.

Fig. 8 shows GOR (a) and DIR (b) as functions of feedwater and air mass flow rates. Maximum GOR occurs with a feedwater mass flow rate near 50 kg/h, which is lower than the optimal operational range in terms of maximising freshwater production. In other words, maximising the GOR does not mean a maximum distillate production. DIR is a better performance indicator because it has a stronger correlation with maximum output. The maximum DIR is approximately 0.44 kg of distillate per kWh.

4.3. Performance parameter analysis

This section addresses an analysis of the HDH system behaviour based on the performance parameters defined in Section 3.4. The ability to produce distillate in a humidification–dehumidification process in a closed air loop depends on the temperature difference between the hot air flow leaving the humidifier, and the cold air stream leaving the dehumidifier. As this temperature difference increases, the circulating air increases its capacity to transport water. The higher air temperature is directly related to the temperature of the water flow feeding the humidifier, which is conditioned on the solar collector's efficiency and incident solar irradiation. The higher air temperature depends on the HDH system feeding water temperature.
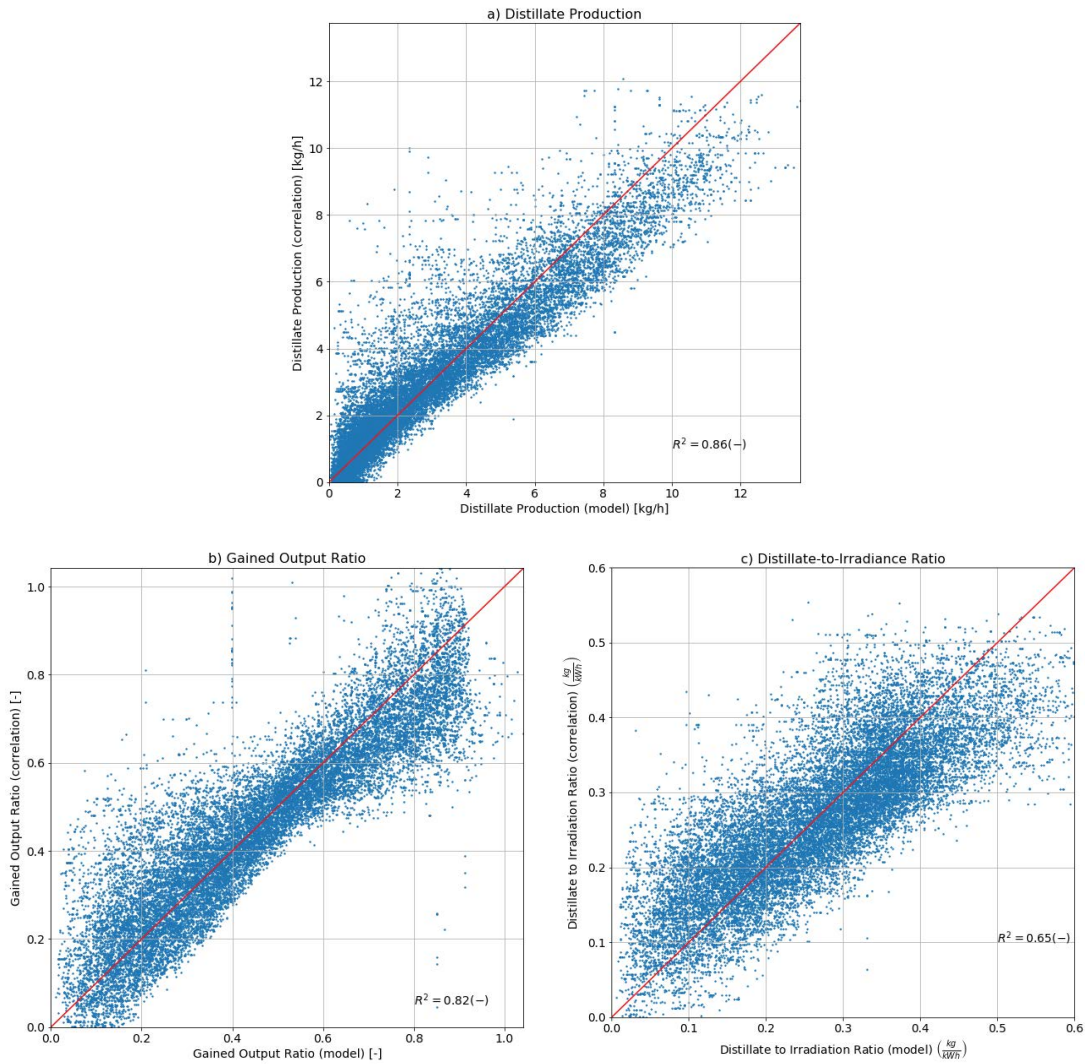
Fig. 6. Correlations for distillate production (a), gained output ratio (b), and distillate-to-irradiance ratio (c). Blue dots are predicted output using the correlations (vertical axis) vs. numerical model output (horizontal axis).
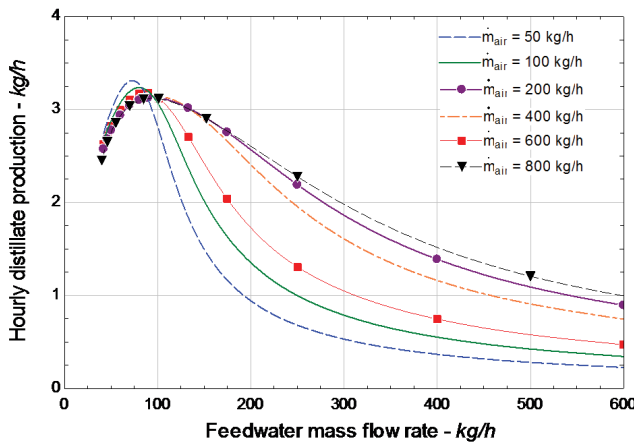

Fig. 7. Distillate production as a function of feedwater mass flow rate for different air mass flow rates.

Fig. 9 shows the relation between the two main conventional desalination parameters, GOR and RR, for different water-temperature difference ΔT between ΔT = 30 to 70 K. The ΔT is given by the difference between the temperature of the water flow feeding the humidifier and the water temperature feeding the HDH system. As both GOR and RR are performance parameters for the desalination subunit, the relation between them does not depend on solar irradiance and solar collectors performance. As stated in the previous section, the DIR is proposed as a better performance parameter than GOR for solar desalination units; consequently, the relation between DIR and RR is presented in Fig. 10. The DIR-RR plot shows that the distillate production increases as the water's temperature difference also increases because of the air's capacity to transport water, similar to the GOR-RR plot. The irradiance intensity has some impact on the recovery ratio and, in consequence, in distillate production. The solar irradiance has a more substantial influence on DIR and RR as the water's temperature difference is higher because increasing
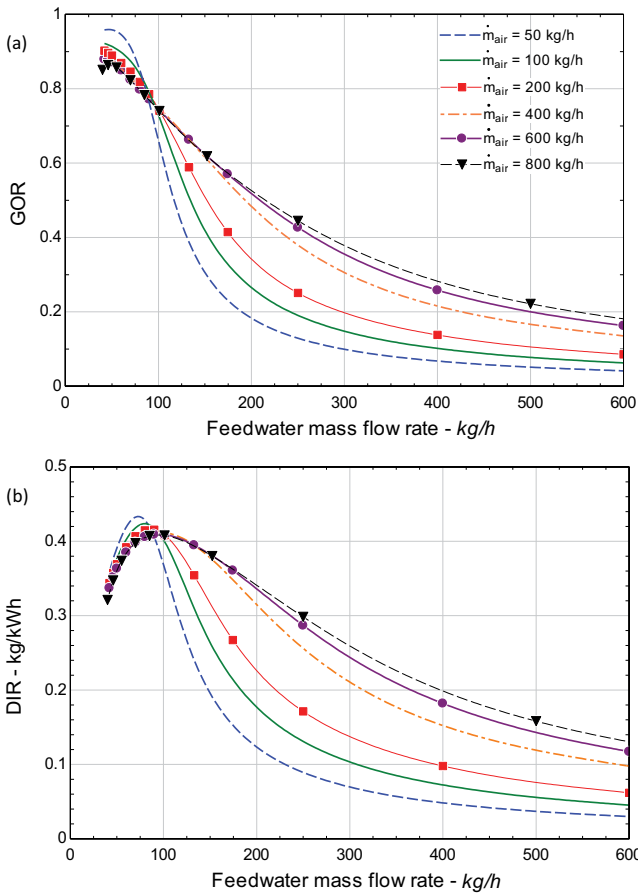
Fig. 8. (a) Gained output ratio (GOR) and (b) distillate-to-irradiance ratio (DIR) as a function of feedwater and air mass flow rates.
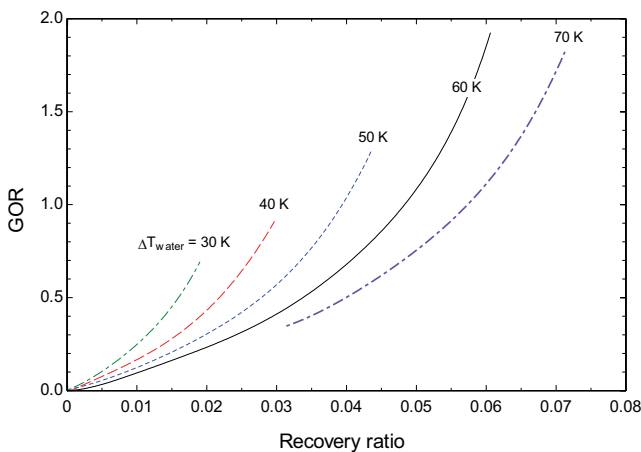

Fig. 9. Relation between GOR and RR for various HDH water temperature differences.

water's ΔT requires reducing the feedwater mass flow rate. Consequently, the solar collector operates at a higher temperature, which implies a lower collector efficiency, as the cooling capacity is reduced. Therefore, as solar irradiation increases, a higher collector temperature is achieved, which gives a lower distillation production.
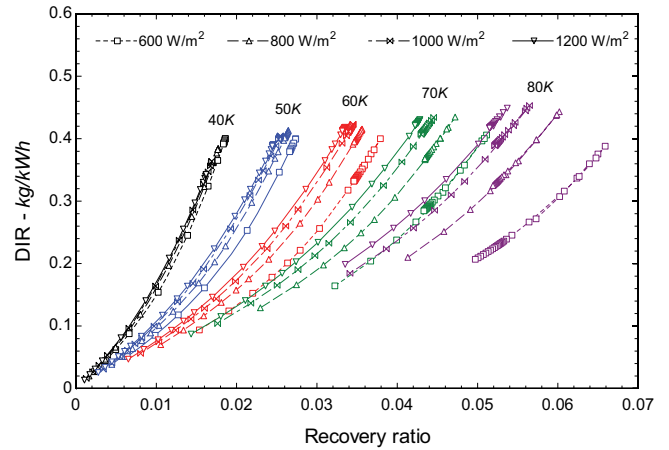

Fig. 10. Relation between DIR and RR for different solar irradiance (markers) and feedwater temperature difference (line colors).

The DIR, and therefore the distillate production, depends on the water temperature difference and solar irradiance. Also, as it was shown in section 4.2, the production relies on the mass ratio (MR). DIR's isolines can be obtained for different irradiance and MR conditions. Fig. 11 presents these contour curves for four different HDH water temperature differences (50, 60, 70, and 80 K). In each plot, a red line shows the maximum production curve. These figures suggest that for a given irradiance, there is a specific MR that determines the maximum distillate production. The lower the water temperature difference, the smaller the MR, to ensure maximum output. Also, this suggests that the water temperature difference determines the maximum DIR, with a slight influence of the irradiance. For 50 K, the maximum DIR is near 0.4 kg/kWh, increasing until a maximum of 0.45 kg/kWh for 80 K.

These charts can be used as an operation control to determine the optimal MR for some given environmental conditions. Given a solar irradiance and a temperature difference, the required MR could be obtained through these charts ensuring maximum production, and the estimated distillate production (M_d) can be determined from DIR through Eq. (19).

4.4. Geographical influence

The geographical influence is assessed by the simulation of the system in different locations of Chile, during a typical meteorological year (TMY). The sites are chosen considering the available data for the superficial sea temperature (TSM) provided by the Chilean Naval Hydrographic Service (SHOA) [51]. The radiation and ambient temperature data are extracted from Sarmiento [52] and Universidad de Chile's Explorador Climático platform [53], respectively. The environmental variables are processed to obtain synthetic weather data in a similar manner as described in Saldivia et al. [8], which is based on Knight et al. [54] and Duffie and Beckman [48] procedures. Table 8 shows geographical data and monthly average meteorological data for the chosen locations.
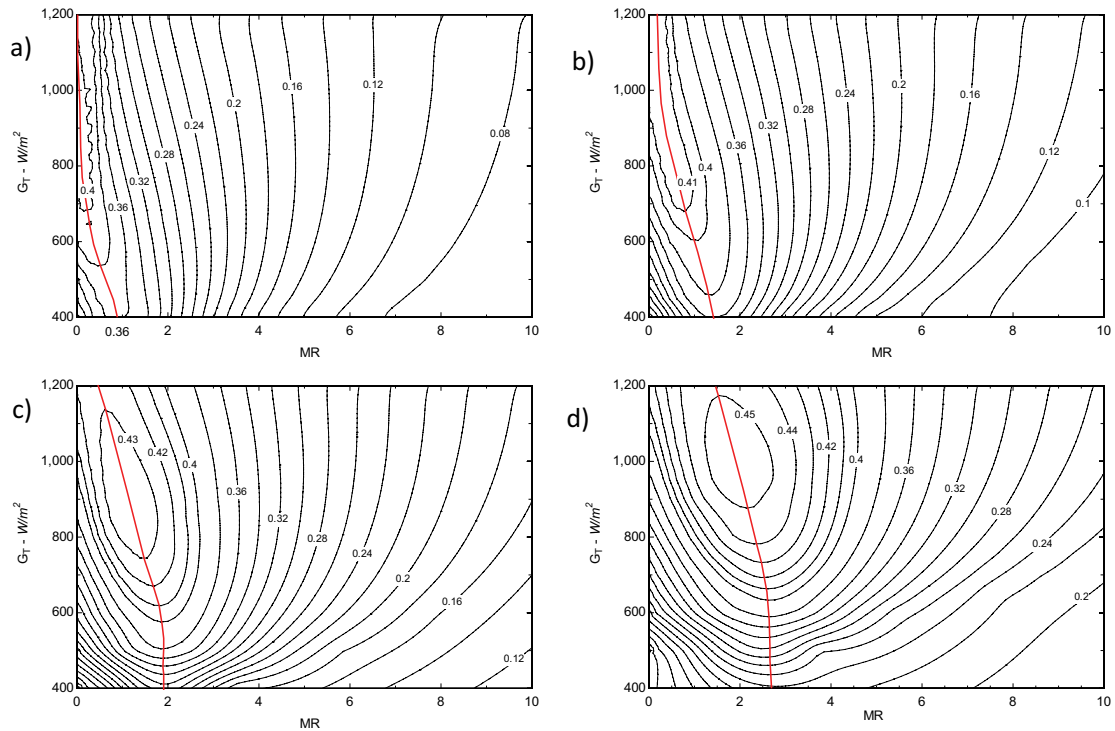
Fig. 11. DIR's level curves as a function of irradiance (G_T) and mass flow rate ratio (MR) for four water temperature differences: (a) 50 K, (b) 60 K, (c) 70 K, and (d) 80 K. Optimum distillate production in the red line.

Table 8
Geographical data, annual average mean temperature, and annual accumulated solar radiation

City	Latitude, °	Longitude, °	Annual accumulated horizontal radiation, MJ/m² y	Annual average mean temperature, °C	Annual average sea temperature, °C
Arica	−18.47	−70.3	6,030	18.6	18.1
Iquique	−20.22	−70.2	6,240	17.9	17.1
Antofagasta	−23.63	−70.4	6,637	16.4	17.7
Caldera	−27.04	−70.5	5,711	15.2	15.6
Valparaíso	−33.07	−71.6	5,089	14.1	14.0
Talcahuano	−36.72	−73.1	5,241	12.1	13.8
Coyhaique	−45.63	−72.1	4,079	8.1	13.8

Data extracted from [51–53].

The monthly accumulated production for four locations is presented in Fig. 12. The seasonal behaviour is clear, having more distillate production during the summer season. Besides, the annual radiation is a crucial parameter in obtaining a high-performance value. The best location, Antofagasta, has 62% more solar radiation and produces 57% more distillate than the worst location, Coyhaique.

Fig. 13a shows the correlation between solar radiation and distillate production, plotted for the seven selected locations. These results indicate a linear trend between these two parameters. In Chile, the solar irradiation varies mainly due to latitude; therefore, it is possible to obtain a relation between production and latitude, which is shown in Fig. 13b. The average ambient temperature and sea

water temperature also have an influence, but their impact seems to be less critical than solar radiation. Eq. (25) shows a multiple linear regression to predict the yearly distillate production as a function of annual average ambient temperature, sea water temperature, and solar radiation with a correlation index R^2 of 0.975.

$$M_d = 0.667\overline{H_h} - 22.4\overline{T_{amb}} + 48.13\overline{T_{sea}} - 692.14 \tag{25}$$

Eq. (25) presents a long-term (annual) distillate production based on all the different weathers present in the Chilean territory. As the final equation only includes the main environmental parameters affecting the HDH facility, it is suggested that this correlation could be extended
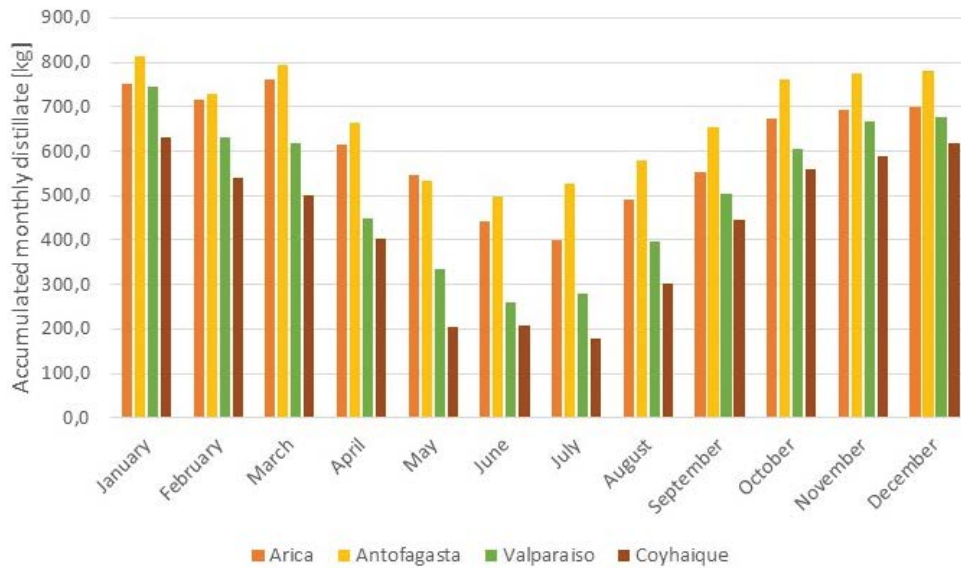
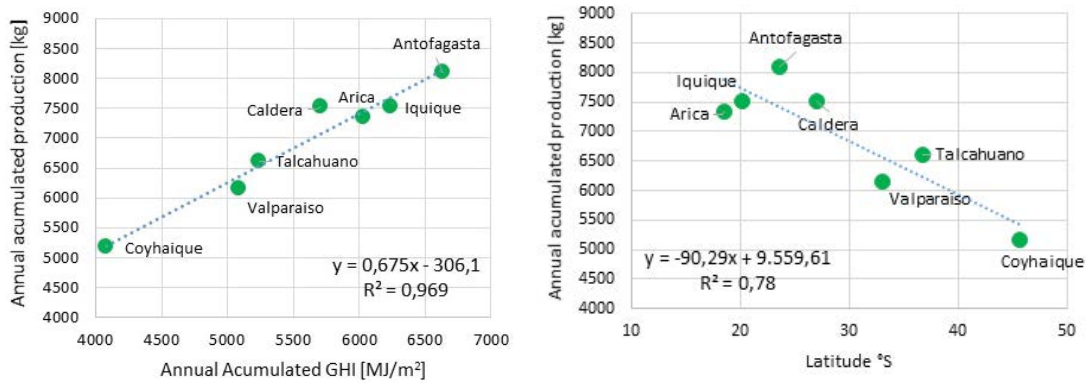Fig. 12. Monthly accumulated distillate production for four locations.

Fig. 13. Relation between annual accumulated production vs. annual accumulated GHI (a) and latitude (b).

to other locations around the world. Therefore, an instantaneous distillate production can be estimated from Eqs. (22)–(24), and long-term production can be obtained from Eq. (25).

5. Conclusions

An autonomous experimental test facility of an HDH desalination system driven by solar energy was built, which is used to develop and validate a numerical model to study different operational conditions. A new performance parameter called DIR is suggested, which is useful to characterise specifically solar thermal desalination systems. This parameter shows to be better than the conventional GOR to identify the optimal operational point under known environmental conditions. In addition, a sensitivity analysis shows that mass flow rates, solar radiation, and ambient temperatures are the key operational parameters. For this configuration, the packed bed and size of the equipment are not considered a constraint if these are well dimensioned. Finally, a long-term correlation to estimate the distillate production based on yearly average environmental parameters (solar radiation, sea water and

ambient temperatures) is developed with a high correlation index. Therefore, through this analysis, it is possible to estimate the distillate production on both short-term [Eq. (22)] and long-term [Eq. (25)] periods, depending on the required analysis.

The experimental facility, the numerical model, and the analysis performed on in this work are powerful tools to support the exploration and development of inexpensive autonomous solutions for the provision of freshwater in small and isolated communities. In further studies, using the numerical model, other operational conditions may be explored, including variable flow rates and equipment size, transient analysis, and energy storage and recovery options. A similar analysis may be expanded to CAOW configuration. Finally, a multistage HDH system is under development, based on the preliminary results shown in this study.

Symbols

a_h	—	Packing specific area, m^2/m^3
A	—	Surface area, m^2
b_f	—	Fin separation, mm
c_p	—	Specific heat, J/kg°C
C	—	Heat capacitance, J/°C
D	—	Diameter, m
DIR	—	Distillate-to-irradiance ratio, –
e	—	Thickness, m
F_R	—	Heat removal factor, –
G_T	—	Global radiation, W/m^2
GOR	—	Gained output ratio, –
h	—	Heat transfer coefficient, $W/m^2°C$
h_D	—	Mass transfer coefficient, $kg/s–m^2$
H	—	Height, m
H_h	—	Monthly horizontal irradiation, J/m^2
i	—	Enthalpy, J/kg
L	—	Length, m
M, m	—	Mass flow, kg/s
MR	—	Mass ratio, –
N	—	Number, –
RR	—	Recovery ratio, –
Q	—	Heat flow, W
S_i, S_{ij}, S_T	—	Sobol method indexes
T	—	Temperature, °C
t	—	Time, s
U	—	Overall heat transfer coefficient, W/m^2
U_L	—	Overall heat loss coefficient, W/m^2
V	—	Volume, m^3
W	—	Width, m
Z	—	Height, m

Greeks

ρ	—	Density, kg/m^3
λ	—	Latent heat of vaporization, J/kg
μ	—	Rugosity, mm
ω	—	Absolute humidity, kg/kg
(τα)	—	Transmission-absorption coeff., –

Suffixes

a	—	Dry air
aw	—	Humid air
amb	—	Ambient
c	—	Convection, condenser
C	—	Collector
d	—	Distillate
exp	—	Experimental
f	—	Flow, collector water flow, fin
fw	—	Feedwater (inlet seawater)
h	—	Humidifier
hp	—	Humidifier packing
hx	—	Heat exchanger
i	—	Specific hour, index
j	—	Dehumidifier pass
m	—	Mass transfer
o, out	—	Out, outside, outer
p	—	Passes, pipe
PV	—	Photovoltaic panel
r	—	Rows
s	—	Saturated condition
sea	—	Sea
sim	—	Simulation
sol	—	Solar
st	—	Storage tank
T	—	Total
u	—	Useful heat (from collectors)
v	—	Vapor
w	—	Water

References

[1] J.E. McMahon, S.K. Price, Water and energy interactions, Annu. Rev. Environ. Resour., 36 (2011) 163–191.

[2] A. Endo, I. Tsurita, K. Burnett, P.M. Orencio, A review of the current state of research on the water, energy, and food nexus, J. Hydrol.: Reg. Stud., 11 (2017) 20–30.

[3] N. Ghaffour, J. Bundschuh, H. Mahmoudi, M.F.A. Goosen, Renewable energy-driven desalination technologies: a comprehensive review on challenges and potential applications of integrated systems, Desalination, 356 (2015) 94–114.

[4] A/RES/70/1 Transforming Our World: The 2030 Agenda for Sustainable Development, Department of Economic and Social Affairs Sustainable Development, United Nations, 2030.

[5] A. Guterres, The Sustainable Development Goals Report 2017, United Nations, New York, 2017. Available at: https://unstats.un.org/sdgs/files/report/2017/TheSustainableDevelopmentGoalsReport2017.pdf

[6] S. Herrera-León, C. Cruz, A. Kraslawski, L.A. Cisternas, Current situation and major challenges of desalination in Chile, Desal. Water Treat., 171 (2019) 93–104.

[7] Anuario Estadístico de Energía 2019, Comisión Nacional de Energía', 2019.

[8] D. Saldivia, C. Rosales, R. Barraza, L. Cornejo, Computational analysis for a multi-effect distillation (MED) plant driven by solar energy in Chile, Renewable Energy, 132 (2019) 206–220.

[9] H. Sharon, K.S. Reddy, A review of solar energy driven desalination technologies, Renewable Sustainable Energy Rev., 41 (2015) 1080–1118.

[10] M. Shatat, M. Worall, S. Riffat, Opportunities for solar water desalination worldwide: review, Sustainable Cities Soc., 9 (2013) 67–80.

[11] C. Li, Y. Goswami, E. Stefanakos, Solar assisted sea water desalination: a review, Renewable Sustainable Energy Rev., 19 (2013) 136–163.

[12] G.P. Narayan, M.H. Sharqawy, E.K. Summers, J.H. Lienhard, S.M. Zubair, M.A. Antar, The potential of solar-driven humidification–dehumidification desalination for small-scale decentralized water production, Renewable Sustainable Energy Rev., 14 (2010) 1187–1201.

[13] E. Mathoulakis, V. Belessiotis, E. Delyannis, Desalination by using alternative energy: review and state of the art, Desalination, 203 (2007) 346–365.

[14] M.T. Ali, H.E.S. Fath, P.R. Armstrong, A comprehensive techno-economical review of indirect solar desalination, Renewable Sustainable Energy Rev., 15 (2011) 4187–4199.

[15] A.E. Kabeel, M.H. Hamed, Z.M. Omara, S.W. Sharshir, Water desalination using a humidification–dehumidification technique—a detailed review, Nat. Resour., 4 (2013) 286–305.

[16] W. Abdelmoez, M.S. Mahmoud, T.E. Farrag, Water desalination using humidification–dehumidification (HDH) technique powered by solar energy: a detailed review, Desal. Water Treat., 52 (2014) 4622–4640.

[17] Y. Zhang, M. Sivakumar, S. Yang, K. Enever, M. Ramezanianpour, Application of solar energy in water treatment processes: a review, Desalination, 428 (2018) 116–145.

[18] K. Srithar, T. Rajaseenivasan, Recent fresh water augmentation techniques in solar still and HDH desalination – a review, Renewable Sustainable Energy Rev., 82 (2018) 629–644.

[19] R. Santosh, T. Arunkumar, R. Velraj, G. Kumaresan, Technological advancements in solar energy driven humidification–dehumidification desalination systems – a review, J. Cleaner Prod., 207 (2019) 826–845.

[20] A. Kasaeian, S. Babaei, M. Jahanpanah, H. Sarrafha, A. Sulaiman Alsagri, S. Ghaffarian, W.-M. Yan, Solar humidification–dehumidification desalination systems: a critical review, Energy Convers. Manage., 201 (2019) 112129, doi: 10.1016/j.enconman.2019.112129.

[21] J. Chen, D. Han, W. He, Y. Liu, J. Gu, Theoretical and experimental analysis of the thermodynamic and economic performance for a packed bed humidifier, Energy Convers. Manage., 206 (2020) 112497, doi: 10.1016/j.enconman.2020.112497.

[22] K. Zhani, H. Ben Bacha, Experimental investigation of a new solar desalination prototype using the humidification–dehumidification principle, Renewable Energy, 35 (2010) 2610–2617.

[23] C. Yamalı, İ. Solmus, A solar desalination system using humidification–dehumidification process: experimental study and comparison with the theoretical results, Desalination, 220 (2008) 538–551.

[24] J.C. Kloppers, D.G. Kröger, A critical investigation into the heat and mass transfer analysis of counterflow wet-cooling towers, Int. J. Heat Mass Transfer, 48 (2005) 765–777.

[25] T. Rajaseenivasan, K. Srithar, Potential of a dual purpose solar collector on humidification–dehumidification desalination system, Desalination, 404 (2017) 35–40.

[26] K. Srithar, T. Rajaseenivasan, Performance analysis on a solar bubble column humidification–dehumidification desalination system, Process Saf. Environ. Prot., 105 (2017) 41–50.

[27] C. Yıldırım, İ. Solmuş, A parametric study on a humidification–dehumidification (HDH) desalination unit powered by solar air and water heaters, Energy Convers. Manage., 86 (2014) 568–575.

[28] W. Gang, H. Zheng, H. Kang, Y. Yang, P. Cheng, Z. Chang, Experimental investigation of a multi-effect isothermal heat with tandem solar desalination system based on humidification–dehumidification processes, Desalination, 378 (2016) 100–107.

[29] C. Muthusamy, K. Srithar, Energy and exergy analysis for a humidification–dehumidification desalination system integrated with multiple inserts, Desalination, 367 (2015) 49–59.

[30] S.W. Sharshir, G. Peng, N. Yang, M.A. Eltawil, M.K.A. Ali, A.E. Kabeel, A hybrid desalination system using humidification–dehumidification and solar stills integrated with evacuated solar water heater, Energy Convers. Manage., 124 (2016) 287–296.

[31] W.F. He, D. Han, W.P. Zhu, C. Ji, Thermo-economic analysis of a water-heated humidification–dehumidification desalination system with waste heat recovery, Energy Convers. Manage., 160 (2018) 182–190.

[32] W.F. He, J.J. Chen, M.R. Zhen, D. Han, Thermodynamic, economic analysis and optimization of a heat pump driven desalination system with open-air humidification–dehumidification configurations, Energy, 174 (2019) 768–778.

[33] A.E. Kabeel, E.M.S. El-Said, A hybrid solar desalination system of air humidification–dehumidification and water flashing evaporation: Part II. Experimental investigation, Desalination, 341 (2014) 50–60.

[34] A.E. Kabeel, M. Abdelgaied, Experimental evaluation of a two-stage indirect solar dryer with reheating coupled with HDH desalination system for remote areas, Desalination, 425 (2018) 22–29.

[35] A.E. Kabeel, M. Abdelgaied, Y. Zakaria, Performance evaluation of a solar energy assisted hybrid desiccant air conditioner integrated with HDH desalination system, Energy Convers. Manage., 150 (2017) 382–391.

[36] R. Branke, T.P. Fluri, P.V. Lefort, Combining concentrating solar power with multiple effect distillation at inland locations – an economically viable option for Northern Chile?, AIP Conf. Proc., 2033 (2018) 160001, doi: 10.1063/1.5067160.

[37] C. Mata-Torres, R.A. Escobar, J.M. Cardemil, Y. Simsek, J.A. Matute, Solar polygeneration for electricity production and desalination: case studies in Venezuela and northern Chile, Renewable Energy, 101 (2017) 387–398.

[38] C. Mata-Torres, A. Zurita, J.M. Cardemil, R.A. Escobar, Exergy cost and thermoeconomic analysis of a Rankine Cycle + Multi-Effect Distillation plant considering time-varying conditions, Energy Convers. Manage., 192 (2019) 114–132.

[39] C. Valenzuela, C. Mata-Torres, J.M. Cardemil, R.A. Escobar, CSP + PV hybrid solar plants for power and water cogeneration in northern Chile, Sol. Energy, 157 (2017) 713–726.

[40] C. Mata-Torres, P. Palenzuela, A. Zurita, J.M. Cardemil, D.C. Alarcón-Padilla, R.A. Escobar, Annual thermoeconomic analysis of a Concentrating Solar Power + Photovoltaic + Multi-Effect Distillation plant in northern Chile, Energy Convers. Manage., 213 (2020) 112852, doi: 10.1016/j.enconman.2020.112852.

[41] F. Suárez, R. Urtubia, Tackling the water-energy nexus: an assessment of membrane distillation driven by salt-gradient solar ponds, Clean Technol. Environ. Policy, 18 (2016) 1697–1712.

[42] J.A. Andrés-Mañas, P. Palenzuela, L. Cornejo, D.C. Alarcón-Padilla, G. Acién, G. Zaragoza, Preliminary evaluation of the use of vacuum membrane distillation for the production of drinking water in Arica (Chile), Desal. Water Treat., 61 (2017) 160–169.

[43] C. Hernández, M. Reyes, R. Barraza, U. Rheinschmidt, D. Saldivia, R. Vasquez-Padilla, Experimental and numerical evaluation of a humidification–dehumidification desalination unit driven by solar energy, AIP Conf. Proc., 2033 (2018) 160003, doi: 10.1063/1.5067162.

[44] S.A. Klein, Engineering Equation Solver, F-Chart Software, 2017.

[45] G. Nellis, S.A. Klein, Heat Transfer, 1 paperback ed., Cambridge University Press, Cambridge, 2012.

[46] F. Bosnjakovic, Technische Thermodynamik, Verlag Theodor Steinkopff, 1965.

[47] R.W. Hyland, A. Wexler, Formulations for thermodymnamic properties of the saturated phases of H_2O from 173.15K to 473.15K, Ashrae Trans. A, 2 (1983) 500–513.

[48] J.A. Duffie, W.A. Beckman, Solar Engineering of Thermal Processes, 4th ed., John Wiley & Sons, Inc., Hoboken, New Jersey, 2013.

[49] I.M. Sobol', Global sensitivity indices for nonlinear mathematical models and their Monte Carlo estimates, Math. Comput. Simul., 55 (2001) 271–280.

[50] A. Saltelli, P. Annoni, I. Azzini, F. Campolongo, M. Ratto, S. Tarantola, Variance based sensitivity analysis of model output. Design and estimator for the total sensitivity index, Comput. Phys. Commun., 181 (2010) 259–270.

[51] SHOA, Servicio Hidrografico y Oceanografico de la Armada, Temperatura Superficial del Mar (TSM), 2018. Available at: http://www.shoa.cl/servicios/TSM/tsm.php

[52] P. Sarmiento, Registro Solarimétrico: Irradiancia Solar en Territorios de la República de Chile, CNE/PNUD/UTFSM, 2008.

[53] (CR)2, Explorador Climático, Centro de la Ciencia del Clima y Resilencia (CR)2, n.d. Available at: http://explorador.cr2.cl/ (accessed July 6, 2020).

[54] K.M. Knight, S.A. Klein, J.A. Duffie, A methodology for the synthesis of hourly weather data, Sol. Energy, 46 (1991) 109–120.